

Explosion Source Strong Ground Motions in the Mississippi Embayment

by Charles A. Langston, Paul Bodin, Christine Powell, Mitch Withers,
Steve Horton, and Walter Mooney

Abstract Two strong-motion arrays were deployed for the October 2002 Embayment Seismic Excitation Experiment to study the spatial variation of strong ground motions in the deep, unconsolidated sediments of the Mississippi embayment because there are no comparable strong-motion data from natural earthquakes in the area. Each linear array consisted of eight three-component K2 accelerographs spaced 15 m apart situated 1.2 and 2.5 km from 2268-kg and 1134-kg borehole explosion sources, respectively. The array data show distinct body-wave and surface-wave arrivals that propagate within the thick, unconsolidated sedimentary column, the high-velocity basement rocks, and small-scale structure near the surface. Time-domain coherence of body-wave and surface-wave arrivals is computed for acceleration, velocity, and displacement time windows. Coherence is high for relatively low-frequency vertical-component Rayleigh waves and high-frequency *P* waves propagating across the array. Prominent high-frequency *PS* conversions seen on radial components, a proxy for the direct *S* wave from earthquake sources, lose coherence quickly over the 105-m length of the array. Transverse component signals are least coherent for any ground motion and appear to be highly scattered. Horizontal phase velocity is computed by using the ratio of particle velocity to estimates of the strain based on a plane-wave-propagation model. The resulting time-dependent phase-velocity map is a useful way to infer the propagation mechanisms of individual seismic phases and time windows of three-component waveforms. Displacement gradient analysis is a complementary technique for processing general spatial-array data to obtain horizontal slowness information.

Introduction

Spatial variation of strong ground motion from earthquakes is an important engineering factor in the design of large structures such as bridges, dams, and pipelines (Hari Chandran and Vanmarcke, 1986; Abrahamson, 1991; Zerva and Zervas, 2002). It is increasingly being recognized that the response of these large structures can be dramatically influenced by whether input loads (ground accelerations) to foundations and piers are coherent or incoherent over the length of the structure. Information on the coherence of the strong-motion wave field can only be determined by using dense arrays of strong-motion accelerographs to record strong ground motions from local earthquakes in active source zones. In fact, much of what is known about the spatial variation of strong ground motions comes from only a few locations in the world, the most notable being the SMART arrays in Taiwan (Abrahamson *et al.*, 1987; see also the review by Zerva and Zervas, 2002), the ROMA array in Mexico City (Bodin *et al.*, 1997; Singh *et al.*, 1997), special experiments associated with sediments in Mexico City (e.g., Barker *et al.*, 1996), and strong-motion arrays in California (e.g., Spudich, 1994).

The New Madrid Seismic Zone (NMSZ) within the Mississippi embayment of the central United States is considered to be an active seismic zone (Nuttli, 1973; Johnston and Schweig, 1996; Tuttle and Schweig, 1999) yet has not suffered a large, destructive earthquake since installation of strong-motion seismographs in the area. A notable characteristic of the NMSZ is the existence of thick, unconsolidated sediments that blanket the area and attain thicknesses of up to 1 km in the Memphis area (Stearns, 1957; Stearns and Marcher, 1962; Self, 1993). The seismic response of these unconsolidated sediments is a major unknown in the evaluation of earthquake hazards due to strong ground motions from earthquakes in the NMSZ (e.g., Bodin and Horton, 1999; Langston *et al.*, 2005). This is a particularly important problem for the area because many major national transportation arteries and pipelines cross or lie near the seismic zone (Langston *et al.*, 2002b).

In October 2002, the Center for Earthquake Research and Information (CERI) at the University of Memphis and the U.S. Geological Survey performed an active source field experiment called the Embayment Seismic Excitation Ex-

periment (ESEE) (Langston *et al.*, 2002a). The experiment was centered about creating seismic waves that traveled almost exclusively within the thick unconsolidated sediments of the embayment through the detonation of two large borehole-emplaced explosions within the sediments. Explosion body and surface waves were recorded by the short-period and broadband stations of the Cooperative New Madrid seismic network, by a temporary deployment of nine broadband stations, and by temporary deployments of a strong ground motion array near each explosion. The primary goal of the experiment was to place bounds on the anelastic attenuation of the sediments by examining the distance decay of the Rayleigh and body waves recorded by the broadband stations. These results are reported elsewhere (Langston *et al.*, 2005).

Chemical explosives were placed in the lower 30 m of 50-m-deep, 20.3-cm (8 inch) steel-cased boreholes. On the night of 29 October 2002 a 1134 kg (2500 lb) single borehole explosion was detonated near Mark Tree, Arkansas (Fig. 1). A 2268 kg (5000 lb), simultaneous two-borehole explosion was detonated the next night near Mooring, Tennessee, near the center of the NMSZ. As part of the experiment we also installed a three-component accelerograph approximately 80 m from each explosion source. Linear arrays of Kinemetrics K2 accelerographs were installed at 2.55 km from the Marked Tree explosion and at 1.2 km from the Mooring explosion (Figs. 1 and 2). Siting for each array was dictated by available agricultural fields near the shot points and by safety and logistical considerations. The array near the Mooring shot point was situated next to the CERI network station, MORT (Mooring, Tennessee).

The strong-motion arrays were installed primarily to investigate the nature of body-wave and surface-wave propagation within the thick unconsolidated sediments of the embayment. The short, linear array geometry was chosen to resolve the horizontal-phase velocity of the high-frequency seismic phases. Although our intent was to examine wave-propagation mechanisms, we realized that the data were the highest-amplitude strong-motion data yet recorded in the NMSZ. Vertical motions at the stations near each blast attained peak accelerations greater than $2g$ and peak accelerations at the two arrays were roughly $20\% g$ (200 cm/sec^2).

These unique data represent an opportunity to examine several important attributes of high-frequency strong ground motion in the Mississippi embayment that should be useful to seismic engineering design. We will be estimating the coherence of various seismic waves across the linear arrays to examine the spatial variation of strong ground motions on the Mississippi River floodplain. Although the seismic source is an explosion, aspects of the strong motions can be related to waves radiated by earthquakes. The data show large PS conversions that can be used as a proxy for S waves radiated from an earthquake source. The slowly propagating Rayleigh waves and related scattered coda on horizontal components can be used to measure structural heterogeneity that affect horizontally propagating shear waves. We will

also demonstrate a very simple technique for determining horizontal-phase velocity by using a plane-wave-propagation model that combines the observed particle velocity field and derived displacement gradients. Results from these empirical analyses will be used in a later report to refine velocity models for the sediments of the embayment by using waveform-modeling methods.

Strong-Motion Array Observations

The site of the Marked Tree explosion (1134 kg) was on agricultural land situated within the St. Francis River drainage on the western margin of the Mississippi River floodplain near the town of Marked Tree, Arkansas (Fig. 1). The K2 array was deployed in an unplanted field to the northeast across the central ditch of the flood-control system. The soil surface was clay rich and formed very sticky mud when wet, a major problem on the rainy night of the test. The larger 2268-kg explosion was placed in the first major river meander south of New Madrid, Missouri, at Mooring, Tennessee. Again, because of safety reasons, the site was situated on private agricultural land and the K2 array deployed in a nearby unplanted field that also was the site of MORT, a CERI short-period seismic station. The ground surface at Mooring was sandy and much easier to navigate when wet.

Each element of the array consisted of a Kinemetrics K2 accelerograph that was securely bolted to a large, square ceramic tile. The ground was prepared so the ceramic tile would be in level contact. Metal stakes were driven into the ground to secure each corner of the tile to ensure that the accelerograph would remain in contact with the ground under high acceleration. This installation arrangement appeared to work well because, even for the close-in stations that experienced $2g$ vertical accelerations, it was very difficult to remove the stakes that held the instrument pad down.

Figure 3 summarizes the data collected by the two K2 arrays. The raw acceleration data were collected at a sampling rate of 200 Hz and were corrected for the nominal instrument responses provided by the instrument manufacturer. Three-component velocity and displacement were derived from acceleration through integration and bandpass filtering between 0.1 and 100 Hz. The horizontal-component data were then vector rotated to form radial (away from the source) and transverse (clockwise looking downward) components for analysis and display. A few problems were discovered in the instrument correction process. We found that the fourth element of the array was set at a lower ground-motion threshold that was exceeded by the P -wave arrival for the larger Mooring blast. This is the source of the filter transient seen in the vertical component displacement data in Figure 3.

The data (Fig. 3) show a remarkable succession of body-wave and surface-wave arrivals that appear to be highly correlated across each array and for each displacement component. The vertical components show high-amplitude,

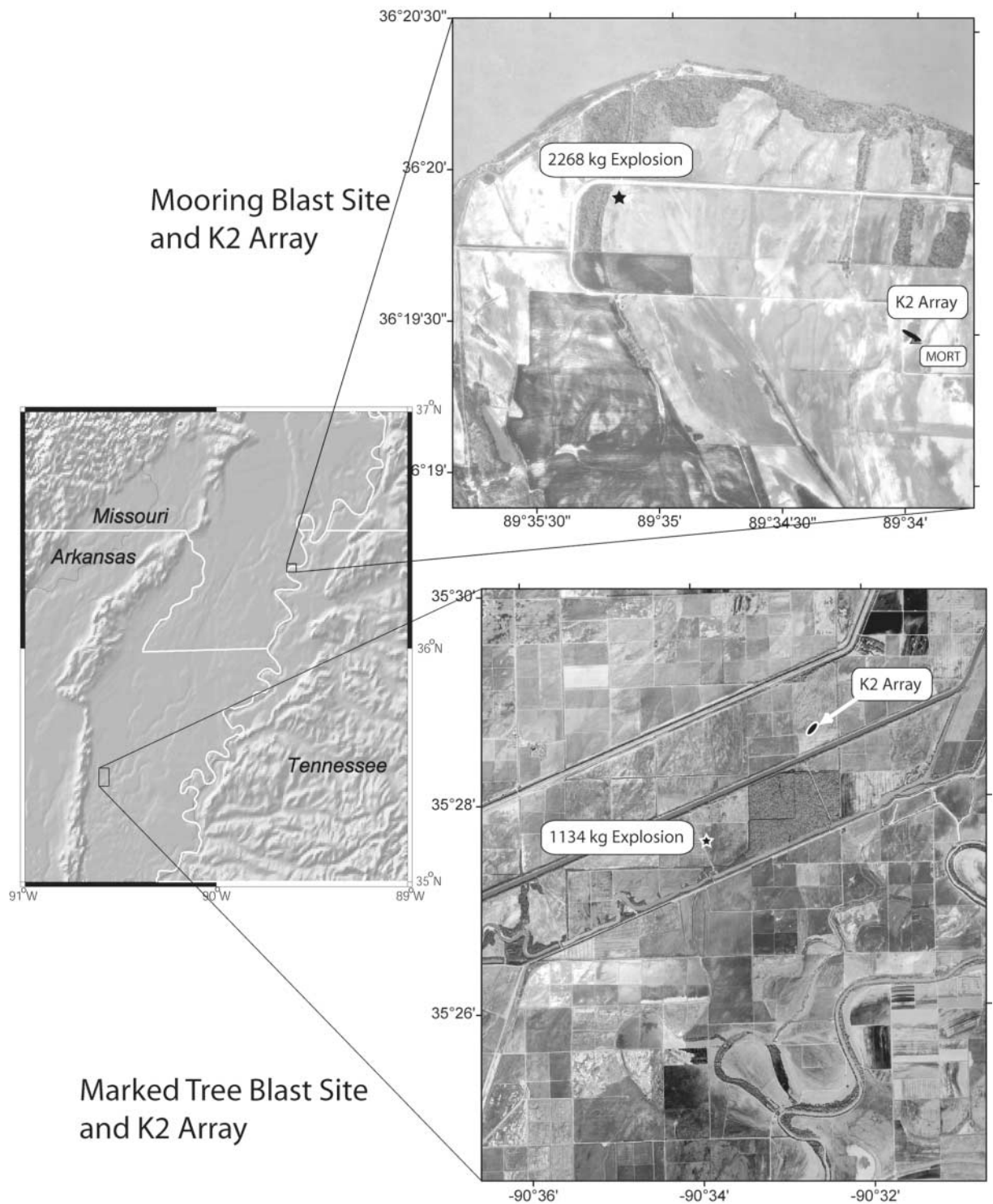


Figure 1. Index map showing the location of Mooring, Tennessee, and Marked Tree, Arkansas explosion sites. Air photos show the location of each ESEE explosion and the location of the K2 accelerograph arrays. Each explosion was situated on private agricultural land.

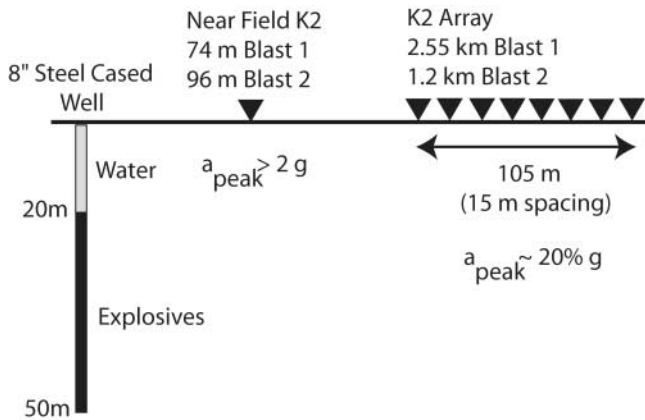


Figure 2. Schematic diagram of the geometry of the explosion sources and location of the strong-motion instrumentation. The location for each K2 array was dictated by logistics near the explosion sources and location of available unused agricultural fields.

high-frequency P -wave arrivals followed by 3- to 4-Hz multimode Rayleigh waves. Radial components show an initial high-frequency set of PS arrivals in the first few seconds followed by a Rayleigh wave train distinctly different from the vertical components. There are also relatively high-amplitude surface-wave-like arrivals late in the coda. Both explosions show the existence of relatively large-amplitude transverse components that are inconsistent with the assumption of an axisymmetric explosion source but are consistent with significant scattering in a heterogeneous structure.

These phase interpretations are based on the integration of travel time, polarization, and phase-velocity analyses of the array data. Figure 4 shows the three-component data for element 8 (the farthest) of each array. Horizontal-phase velocities for several discrete seismic phases were estimated by picking the arrival time of a peak or trough on each array element record and then by fitting the resulting time-distance data with a linear regression algorithm. Phase-velocity estimates are annotated on Figure 4 along with the formal variance of the error from the regression fit. These phase-velocity estimates can be used in conjunction with the known properties of the velocity structure of the unconsolidated sediments to make reasonable hypotheses on the origin of each wave observed in the data. In particular, Langston (2003) produced a reference-velocity model for the unconsolidated sediments based on well log data, earthquake phase-arrival times, and earlier velocity models suggested by Chiu *et al.* (1992), Chen *et al.* (1996), and Liu *et al.* (1997). The important features of this model pertaining to phase interpretations include very low P - and S -wave velocities in the upper 15 m, which will ensure that body-wave ray paths will be near-vertical, an average V_p of about 1.8 km/sec and V_s of 0.6 km/sec for the upper two thirds of the section, and a lower layer associated with Upper Creta-

ceous sediments with a higher V_p of about 2.5 km/sec and V_s of 1.2 km/sec.

An explosion source is primarily a source of P waves. S waves and surface waves are produced because of P -to- S coupling at layer boundaries and the free surface. Each explosion produced an impulsive, high-frequency P wave that is prominent on the vertical components (Figs. 3 and 4). The inferred phase velocities of 1.9 to 2.2 km/sec suggest that these are diving or reflected waves from the base of the sediments. The Marked Tree K2 array was at a greater distance from the source and waveforms show a small, first-arriving P wave with high phase velocity that is interpreted as the refraction in the underlying Paleozoic rocks. Radial components show additional impulsive arrivals within the first 4 sec that are interpreted to be S waves because they are not seen on the vertical components. Their relatively high phase velocities (2.2 to 3 km/sec) suggest that they are S waves converted from P waves in the lower part of the unconsolidated sediments. The lower-frequency waves arriving after 4 sec for both blasts are clearly Rayleigh waves because they have both prograde and retrograde particle motion and are dispersed. Note the very low phase and group velocities for these arrivals. These Rayleigh waves consist of both fundamental- and higher-mode waves; detailed analysis of phase and group velocity showed interference of at least two modes in the time window of 5–10 sec for the Marked Tree data (analysis not shown here).

The transverse component (Figs. 3 and 4) should theoretically be zero for data from an axisymmetric explosion source. There also seem to be significant arrivals at very late times and low apparent group velocity on the radial component as well. Note, for example, that the large radial coda phase at about 16 sec for the Marked Tree blast appears within the array and grows from nearly zero amplitude to almost maximum trace amplitude over the array length. Both of these observations suggest that waves are being scattered by velocity heterogeneity in the embayment sediments. This interpretation is supported by the observation of phase velocities that are comparable to earlier arriving Rayleigh waves for major coda wave trains and by individual arrivals that actually propagate back toward the sources (-700 m/sec arrival on the Marked Tree vertical component near 17 sec, -800 m/sec arrival on the Mooring transverse component on Fig. 4). Also note that the transverse component for the Mooring data is significantly smaller than that for the Marked Tree source, suggesting that the amount of wave scattering increases with distance from the source.

Although these strong-motion seismic waves have been excited from a distinctly non-earthquake-like source, there are aspects of the data that can be examined to obtain information on the coherence and propagation of shear waves. In general, direct S waves from an earthquake in the NMSZ will have horizontal-phase velocities in the range of 2.5 to 3.5 km/sec defined by horizontal-wave propagation in the upper crust. Strong ground motion frequencies of interest are in the 10- to 1-Hz range. The horizontal wavenumber,

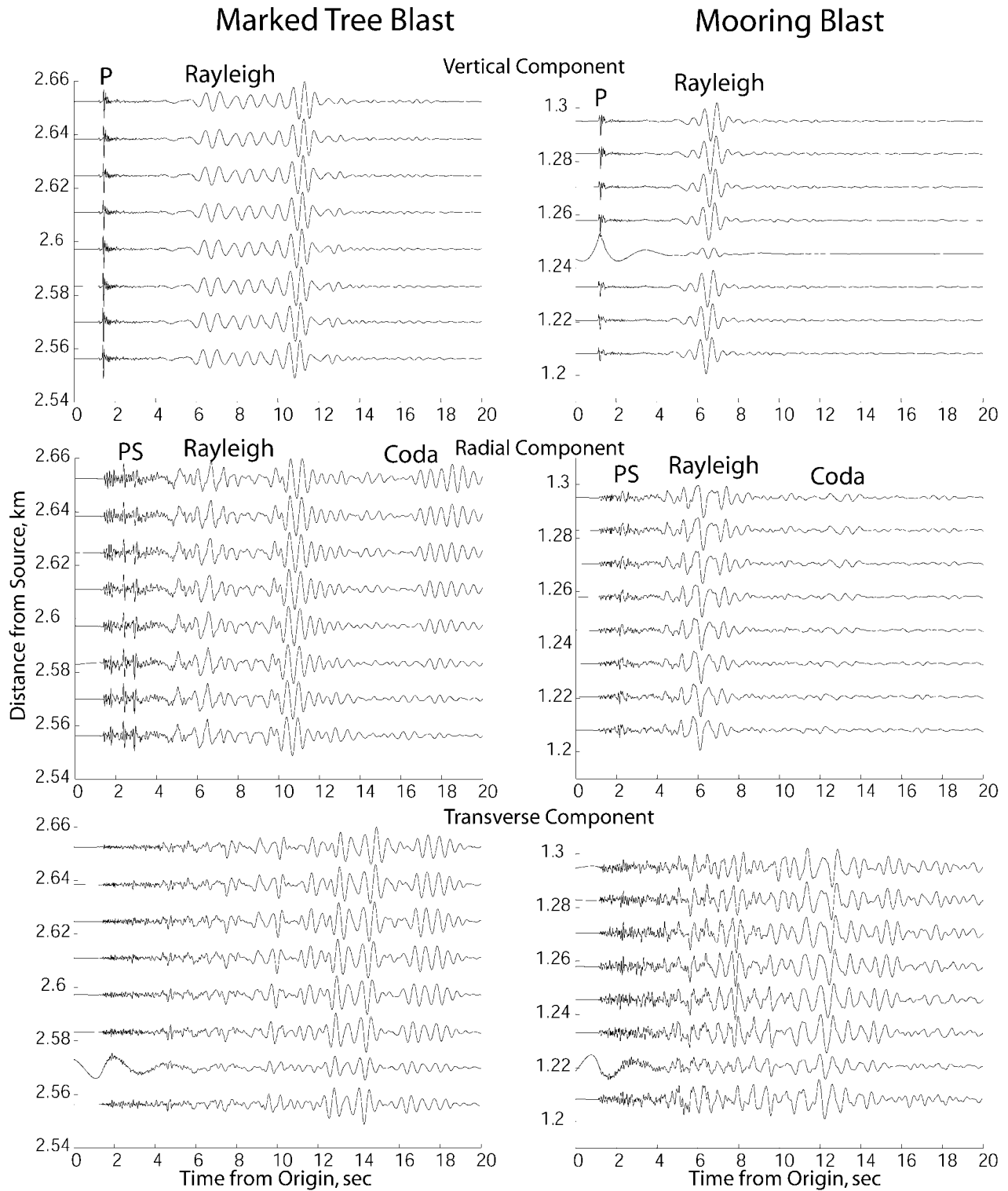


Figure 3. Summary of the array data from each explosion. Major seismic phases are annotated the seismic record sections for each ground-motion component. Ground displacements are shown that were derived from the acceleration data. The plots for each ground-motion component have been normalized. Note the clear body-wave and surface-wave trains.

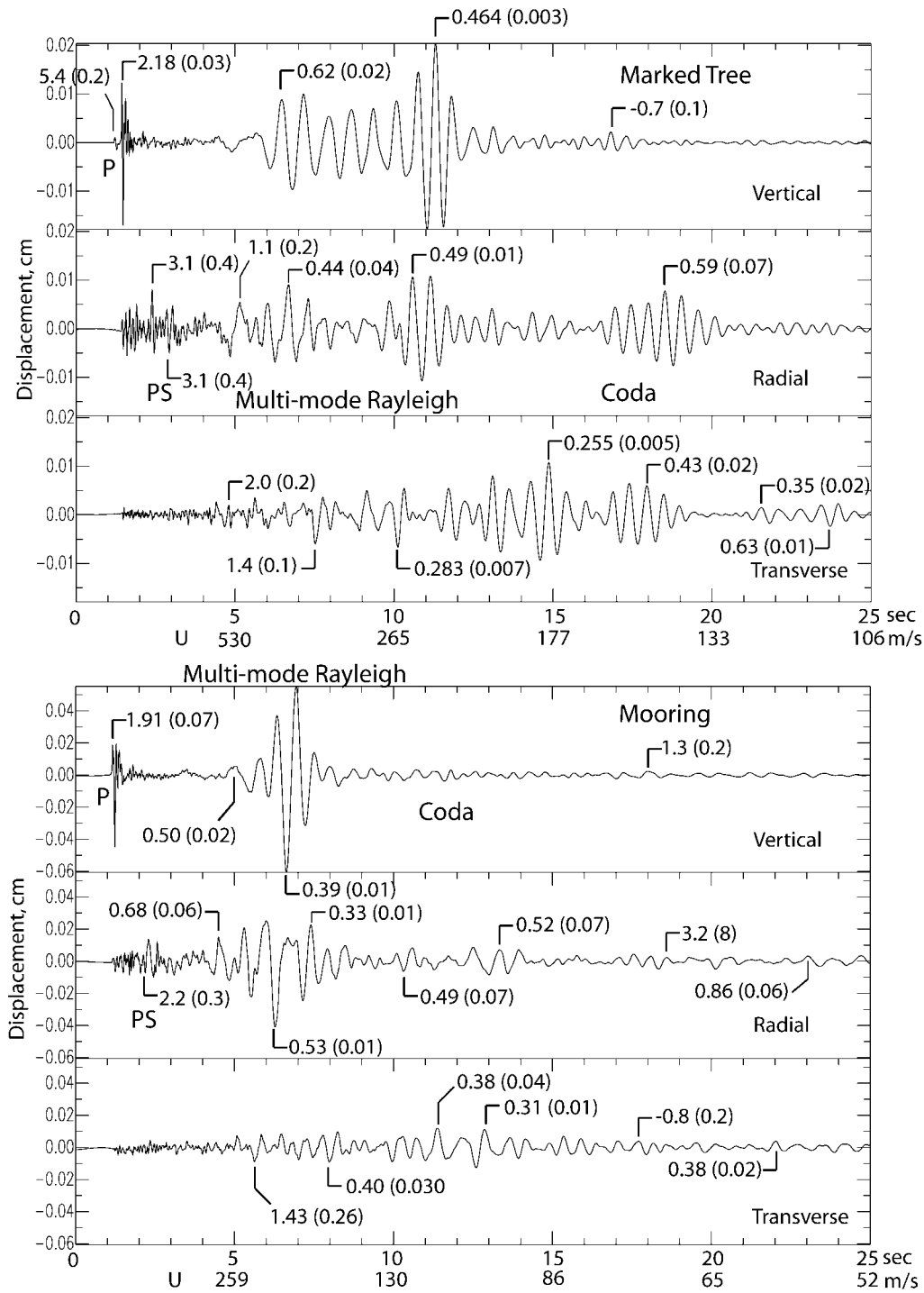


Figure 4. Detail of the three components of displacements shown on a common amplitude scale. Horizontal-phase velocities were determined by using the time move-out of selected phases across each array through linear regression. Phase-velocity values in kilometers per second are shown next to particular phases and the standard error of the determination is in parentheses. Group velocity is also shown under the timescale for each explosion set. Note the very low surface-wave group velocities. Also note that some phase arrivals are negative, denoting propagation toward the source.

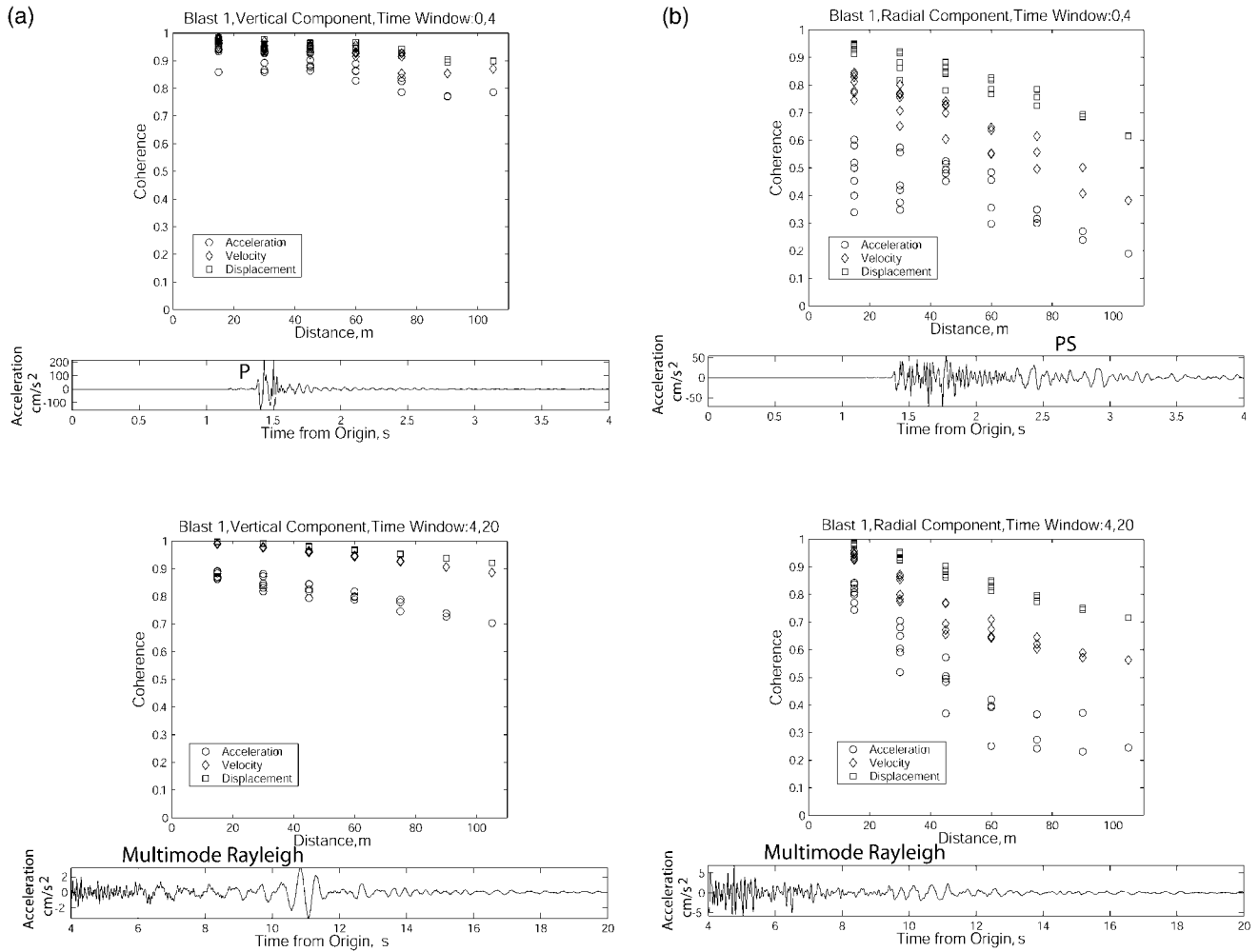


Figure 5. Coherence measurements for two time windows of strong-motion data from the Marked Tree, Arkansas, explosion. The time windows were chosen to isolate the body-wave arrivals (0 to 4 sec) and the surface-wave arrivals (4 to 20 sec). Coherence was computed using equation (2) for each time window and displayed in the plot above the time series. Coherence was measured for all possible combinations of array stations and plotted as a function of interstation distance. Coherence is shown for displacement (squares), velocity (diamonds), and acceleration (circles). Major phases are also annotated. (a) Vertical component. (b) Radial component. (c) Transverse component. (continued)

$k = f/c$, where f is frequency and c is horizontal-phase velocity, will be 4 to 0.3 cycles/km for typical earthquake S waves. The radial component PS conversions have a dominant frequency of about 10 Hz giving a horizontal wavenumber of about 3 cycles/km. The Rayleigh waves have a dominant frequency of about 1–2 Hz giving a horizontal wavenumber of about 2 to 4 cycles/km. Thus, the PS conversions and Rayleigh wave data from the explosion sources have horizontal wavenumbers comparable to expected high-frequency shear waves from earthquakes. We suggest that wave-scattering mechanisms will be similar at these high wavenumbers, justifying using the explosion strong-motion data as a proxy for earthquake strong-motion data.

Coherency and Coherence

Waveform coherency is a function of the physical (spatial and temporal) variation of the wave field and all the practical observational factors involved in measuring the wave field. The composition of the wave field obviously depends on the heterogeneity of the propagation medium along with the heterogeneity of a spatially distributed seismic source (Spudich, 1994; Kramer, 1996; Zerva and Zervas, 2002). Coherency will degrade with position depending on the nature of interference of seismic waves as they radiate from an extended source and the directions and speeds at which they propagate in the medium. Apparent coherency

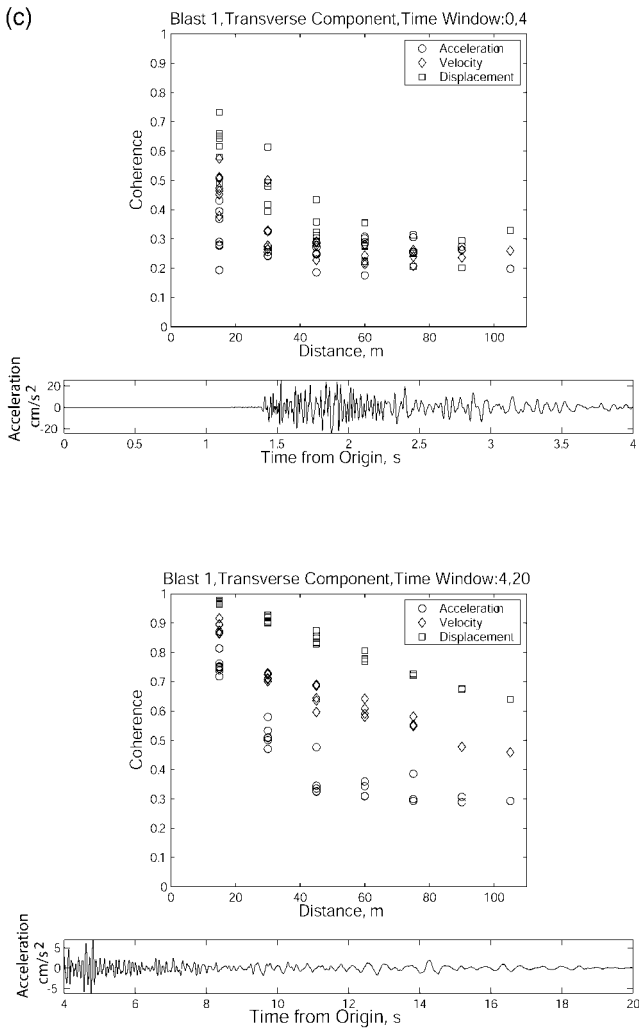


Figure 5. Continued.

degradation can also occur because of seismic instrument response differences and local instrument siting problems, such as how an instrument is coupled to the ground.

Many ways to determine the coherency of multiple time series exist. A standard method that is used in the engineering literature for strong ground motions (e.g., Spudich, 1994; Kramer, 1996; Zerva and Zervas, 2002) is to form the normalized cross-spectral density between the complex Fourier spectra of two time series, say $S_1(\omega)$ and $S_2(\omega)$:

$$S_{12}(\omega) = \frac{S_1(\omega)S_2^*(\omega)}{\sqrt{S_1(\omega)S_1^*(\omega)}\sqrt{S_2(\omega)S_2^*(\omega)}}. \quad (1)$$

In general, the normalized cross-spectral density will have the value of 1 for all frequencies for any two spectra (Zerva and Zervas, 2002). This is avoided in practice by performing spectral averaging over a finite bandwidth to compute the expected value, in the statistical sense, of each spectrum (Spudich, 1994) to estimate coherency. The drawback of

spectral averaging is that the coherency will be a function of the choice of averaging window length. The coherency computed this way is a complex function of frequency. Coherency may be computed from the coherency by taking the modulus and is a real function of frequency because the phase is removed.

We take a pragmatic approach in measuring coherency in the time domain because the data display discrete seismic phases and wave types depending on the choice of time window. Time-domain coherency will be defined using the maximum of the normalized cross correlation:

$$C_{xy} = \frac{\max \int_{-\infty}^{+\infty} x(t)y(t + \tau)dt}{\left(\int_{-\infty}^{+\infty} x^2(t)dt \int_{-\infty}^{+\infty} y^2(t)dt\right)^{1/2}}. \quad (2)$$

This is a natural measure of the similarity of time-domain waveforms that has been used in many source- and structure-modeling studies (e.g., Helmberger, 1983) and is also called the semblance. C_{xy} varies between -1 and $+1$, where a value of $+1$ denotes perfect similarity. Using the maximum of the normalized cross correlation may remove much of the effect of wave passage in degrading the coherence across an array. The effect of wave passage is a well-understood phenomenon in spectral coherency studies (e.g., Spudich, 1994) and is clearly recognized in our data because of the discrete body- and surface-wave phases that propagate across the array. The use of the normalized cross correlation to estimate wave coherence is exactly related to the spectral coherence through the Power theorem of Fourier transforms (see Appendix) where the averaging window is taken across the entire frequency band. Thus, we adopt the use of the term “coherency” in our time-domain measurements as having the same meaning as “coherency” derived by spectral averaging.

The K2 array strong-motion data were cut into two time windows, 0 to 4 sec and 4 to 20 sec, to investigate the coherence of body-wave phases and surface-wave phases. Coherency for a particular ground-motion component was computed for acceleration, velocity, and displacement in the two time windows by taking all possible pairs of array elements. The coherency was then plotted as a function of distance between array elements. Results are shown in Figure 5 for the Marked Tree explosion and Figure 6 for the Mooring explosion.

There is a natural progression to the decrease of coherency with distance. Vertical components of motion (Figs. 5a and 6a) are generally most coherent with distance across the arrays compared with radial (Figs. 5b and 6b) or transverse (Figs. 5c and 6c) motions. Displacement for all ground-motion directions are more coherent than velocities that are, in turn, more coherent than accelerations. This is because displacement, velocity, and acceleration fields contain progressively higher-frequency waves that scatter more with distance. This is demonstrated by the greater relative coherency

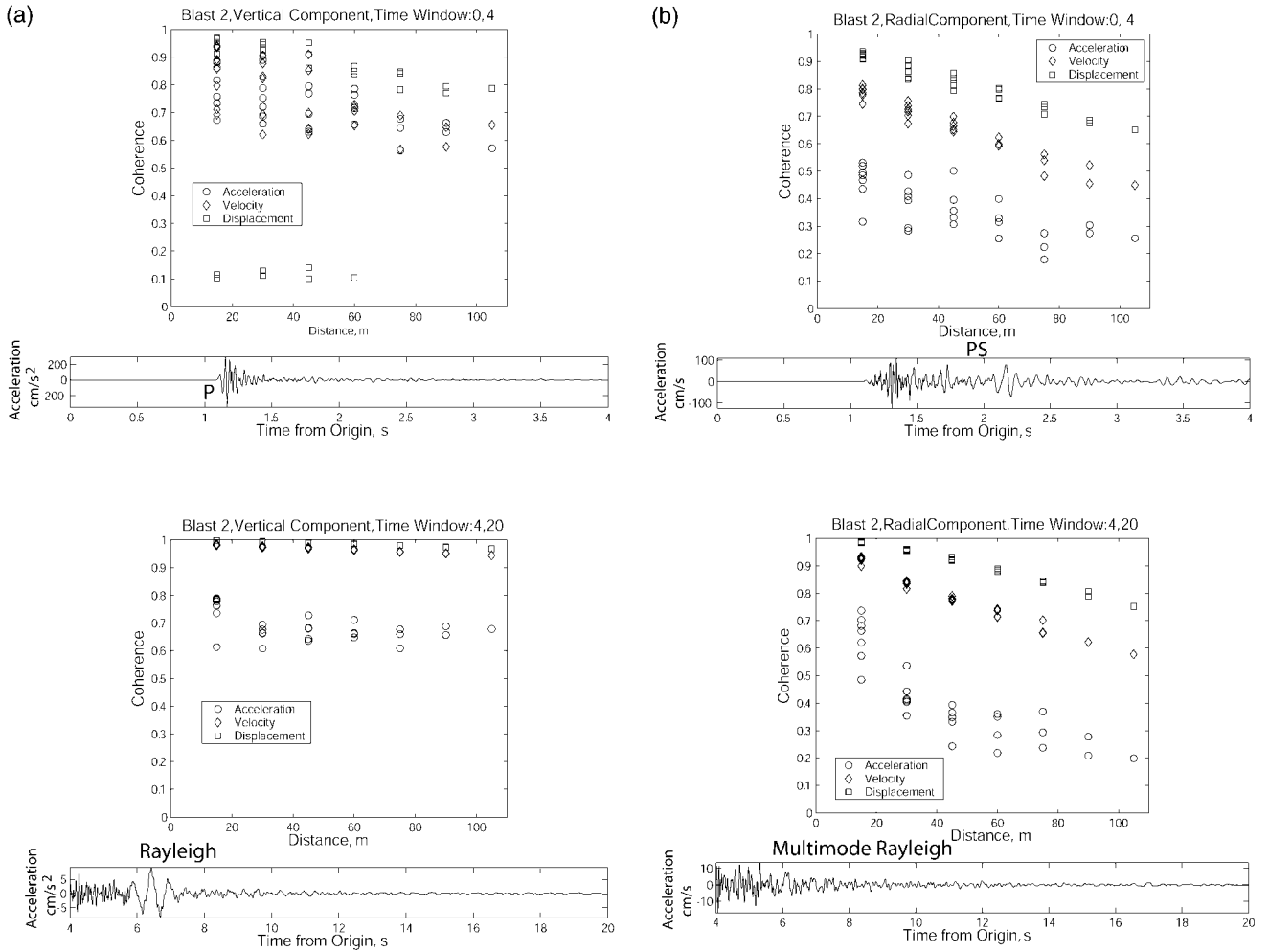


Figure 6. Coherence measurements using the Mooring, Tennessee, array data. Same scheme as in Figure 5. *(continued)*

ence of waves from the Mooring blast that were recorded at 1.2 km compared with waves from the Marked Tree source recorded at 2.6 km. Likewise, coherence is generally greater within the surface-wave windows that contain lower-frequency, longer-wavelength surface-wave phases. Horizontal components reach a coherence floor at about 0.2 for accelerations with transverse accelerations in the 0- to 4-sec time window being least coherent.

The degradation of coherence across these short arrays primarily demonstrates the complexity of high-frequency wave propagation in the heterogeneous structure of flood-plain sediments. Primary waves from the explosion source include *P* and Rayleigh waves that are most coherent on the vertical components. Major converted secondary phases within the structure, such as the radial *PS* waves, appear to clearly propagate across the array but are embedded in a higher-frequency, incoherent coda after the *P* wave. This *P*-wave coda is most clearly seen on the transverse component (0- to 4-sec window; Figs. 5c and 6c) which is direct evidence of high-frequency wave scattering in the structure.

Array Displacement Gradient and Horizontal-Phase Velocity Estimates

An array of matched seismic instruments can be used to compute time-dependent geodetic strain through finite spatial differences of the wave field (Spudich *et al.*, 1995; Bodin *et al.*, 1997; Gomberg *et al.*, 1999). If we define the radial direction with index value 1, the transverse direction with index value 2, and the vertical direction with index value 3, we see that the strains,

$$\varepsilon_{ij} = \frac{1}{2} \left(\frac{\partial u_i}{\partial x_j} + \frac{\partial u_j}{\partial x_i} \right) \quad (3)$$

cannot be completely determined from our linear accelerograph array. We can only determine displacement gradients in the radial, or x_1 , direction. Still, we obtain the axial normal strain as

$$\varepsilon_{11} = \frac{\partial u_1}{\partial x_1} \quad (4)$$

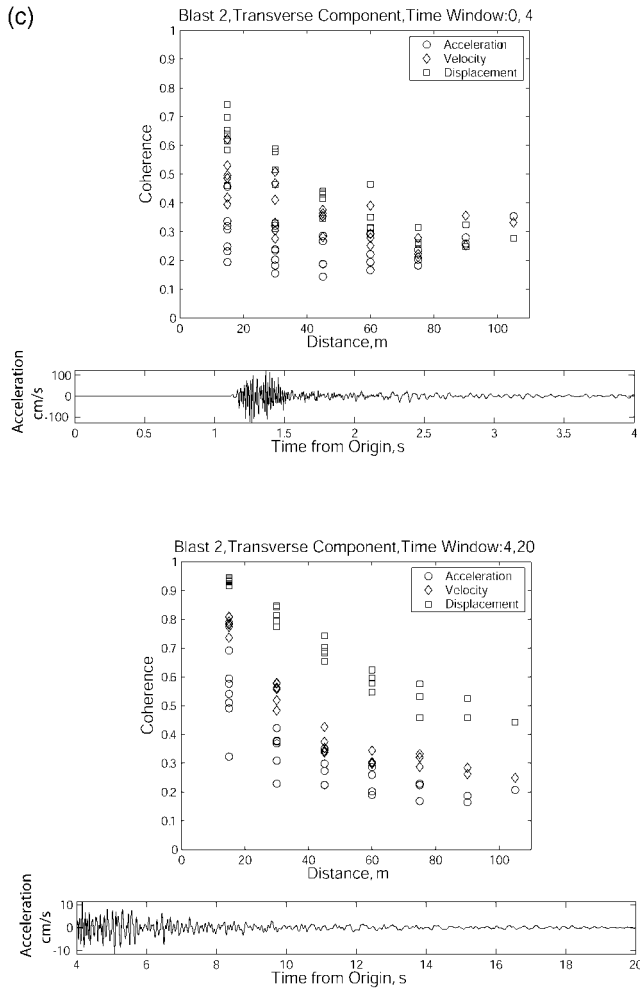


Figure 6. Continued.

and the partial shear strains

$$\begin{aligned} \varepsilon_{12} &\sim \frac{1}{2} \frac{\partial u_2}{\partial x_1} \\ \varepsilon_{13} &\sim \frac{1}{2} \frac{\partial u_3}{\partial x_1} \end{aligned} \quad (5)$$

with the other strains being indeterminate. Ideally, we might expect that the displacement gradient in the transverse direction ($\partial u_i / \partial x_2$) to be close to zero from an axisymmetric explosion source because there should be no azimuthal change in source-radiation pattern. However, vertical-displacement gradients ($\partial u_i / \partial x_3$) should be relatively large for vertically propagating P and S waves within the sediments or for the excitation of surface waves. Furthermore, we suspect from the analysis of coherence that the propagation medium is heterogeneous so that waves are likely propagating in horizontal directions different from x_1 .

Many authors have pointed out the relationship of particle velocity and displacement gradient through a simple

plane-wave model of wave propagation from elementary seismology (e.g., Love, 1927, page 298; Singh *et al.*, 1997; Gomberg *et al.*, 1999). For example, if we have a plane wave propagating along the array in the x_1 direction, the displacement can be represented by

$$u_i = a_i f\left(t - \frac{x_1}{c}\right). \quad (6)$$

The displacement gradient with respect to x_1 is given by

$$\frac{\partial u_i}{\partial x_1} = -\frac{1}{c} \frac{\partial u_i}{\partial t} \quad (7)$$

so that the horizontal-phase velocity can be found from the ratio of the particle velocity to the displacement gradient

$$c = -\frac{\left(\frac{\partial u_i}{\partial t}\right)}{\left(\frac{\partial u_i}{\partial x_1}\right)}. \quad (8)$$

A seismic trace may consist of many plane waves propagating across the array in many different directions. We expect that waves will interfere with each other within any particular time window so that observed displacement gradients and particle velocities will consist of the linear superposition of these waves. The veracity of the plane-wave model of equations (6)–(8) for any particular time window in estimating a single-phase velocity depends on the nature of this interference and whether a single wave dominates the wave field. Intuitively, we expect that large, coherent phases with clear distance moveout will be most amenable to this analysis just as these same phases can be used to infer basic characteristics of the velocity structure by using other techniques.

The displacement gradient may be computed robustly from adjacent receivers of the K2 array by using a simple difference because the highest wavenumbers are ~ 10 cycles/km and interstation distances only 15 m (0.015 km), well within the quarter-wavelength criteria cited by previous investigators (e.g., Bodin *et al.*, 1997). Figure 7 shows an example of the horizontal-displacement gradient computed using stations 4 and 5 from the K2 array that recorded the Marked Tree explosion. The displacement gradients are compared with particle velocity at station 4 to demonstrate the good correlation of waveforms. The difference in relative amplitudes of the observed phases should be related to the differences in phase velocity.

A time-dependent phase-velocity plot can be created by forming the ratio of the particle velocity to the displacement gradient (equation 8). A practical difficulty involves zero crossings of each time series, in particular, the displacement gradient time series because it occurs in the denominator. The envelope function of each time series is computed using

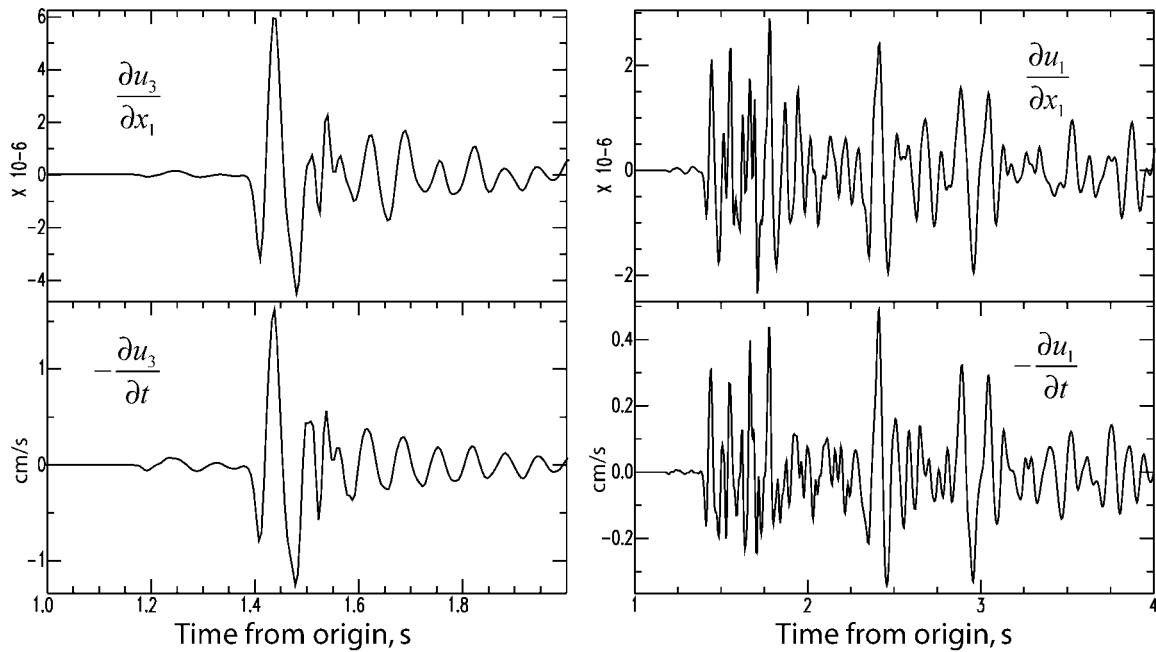


Figure 7. Comparison of the displacement gradients of the vertical (left) and radial (right) displacements with ground velocity for data from the Marked Tree, Arkansas, explosion. The displacement gradient was computed by differencing the waveforms between stations 4 and 5. Ground velocity was computed for station 4. Note the excellent correspondence of waveforms between the two time series. Differences in amplitude reflect phase velocity as given in equation (7).

the modulus of the analytic signal (Farnbach, 1975) and these are used to form the ratio to avoid dividing by zero. Unfortunately, this expedient also removes the directionality inherent in the phase-velocity estimate because positive time-series quantities are used; negative phase velocity (i.e., propagation the other way) will not be detected by using positive-value envelopes.

Figure 8 shows resulting phase-velocity time series for each ground-motion direction of the two K2 arrays. Also shown are the phase-velocity picks for the discrete phases analyzed in Figure 4. In almost every case, the phase velocity determined from travel-time analysis agrees with the phase-velocity estimate from the amplitude analysis. The notable exception occurs for the arrival seen on the transverse component near 10 sec for the Marked Tree explosion (Fig. 8c).

The phase-velocity time series display some general properties for different parts of the seismograms. Major *P*-wave arrivals and *P*-wave coda have relatively high horizontal-phase velocities over the first 4 sec of this high-frequency portion of the waveform. The surface-wave arrivals, coming after 4 sec and continuing until the major vertical Airy phases seen on the vertical components, have characteristically low-phase velocity. However, horizontal-phase velocity seems to be more irregular with higher peaks after about 12 sec for all components. This is the realm of the seismic coda where scattered waves dominate and may arrive from all directions. The horizontal-phase velocity in the radial direction can theoretically be infinite for waves

that illuminate the array perpendicularly from the side. The phase-velocity time series presents another useful view of the wave field that is complementary to standard-array and wave-polarization analyses.

Estimated strains from the two strong-motion arrays range from 10^{-5} to 10^{-6} . These are relatively high seismic strains but are still relatively low for inducing significant nonlinear elastic modulus degradation of unconsolidated and unconfined materials (Vucetic, 1994; Lanzo and Vucetic, 1999).

Discussion

Deployment of these short-aperture arrays was a secondary experiment associated with the ESEE field project and was dictated by available instrumentation, logistics in the field, and the desire to collect phase-velocity information for the propagation of seismic waves in the embayment sediments. The array geometry was very successful in allowing the measurement of arrival-phase velocities to understand the composition of the seismic wave field at short propagation distances. Our present approach of using the array data to investigate displacement gradients and strains would have benefited from a spatially distributed array, however. A two-dimensional array would also allow direct measurement of the azimuth of propagation of the seismic phases to investigate the nature of scattering in the coda and transverse components of motion.

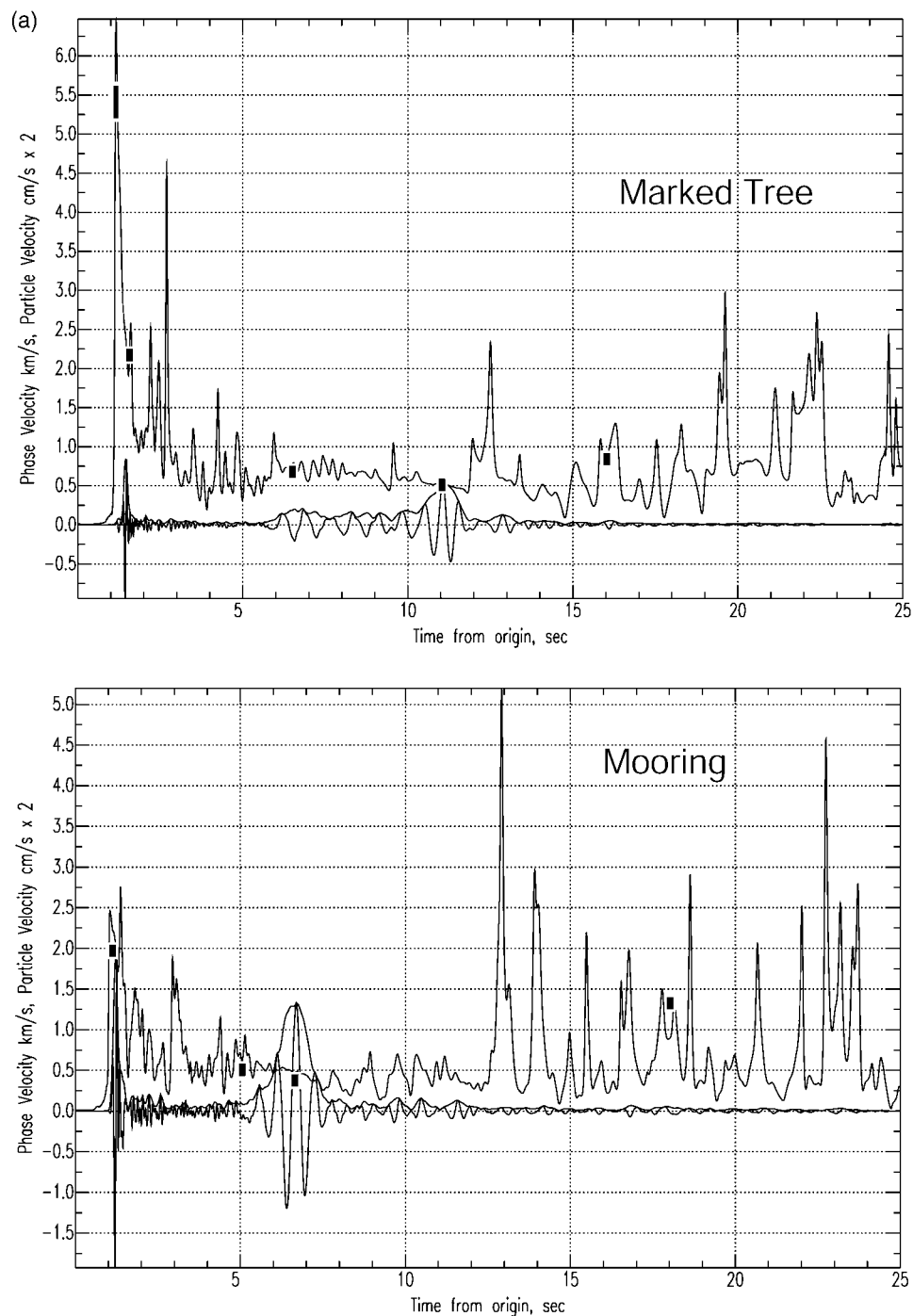


Figure 8. Phase-velocity time series plotted with the envelope of the original ground-velocity data. The filled squares and rectangles represent the value and error of the time-moveout phase-velocity measurements displayed in Figure 4. There is good correspondence between horizontal-phase velocities determined by the independent methods for the major observed phases. Stations 4 and 5 were used to compute displacement gradient and station 5, ground velocity, for the Marked Tree blast. Stations 5 and 6 were used for the Mooring blast. (a) Vertical components for both arrays. (b) Radial components for both arrays. (c) Transverse components for both arrays. *(continued)*

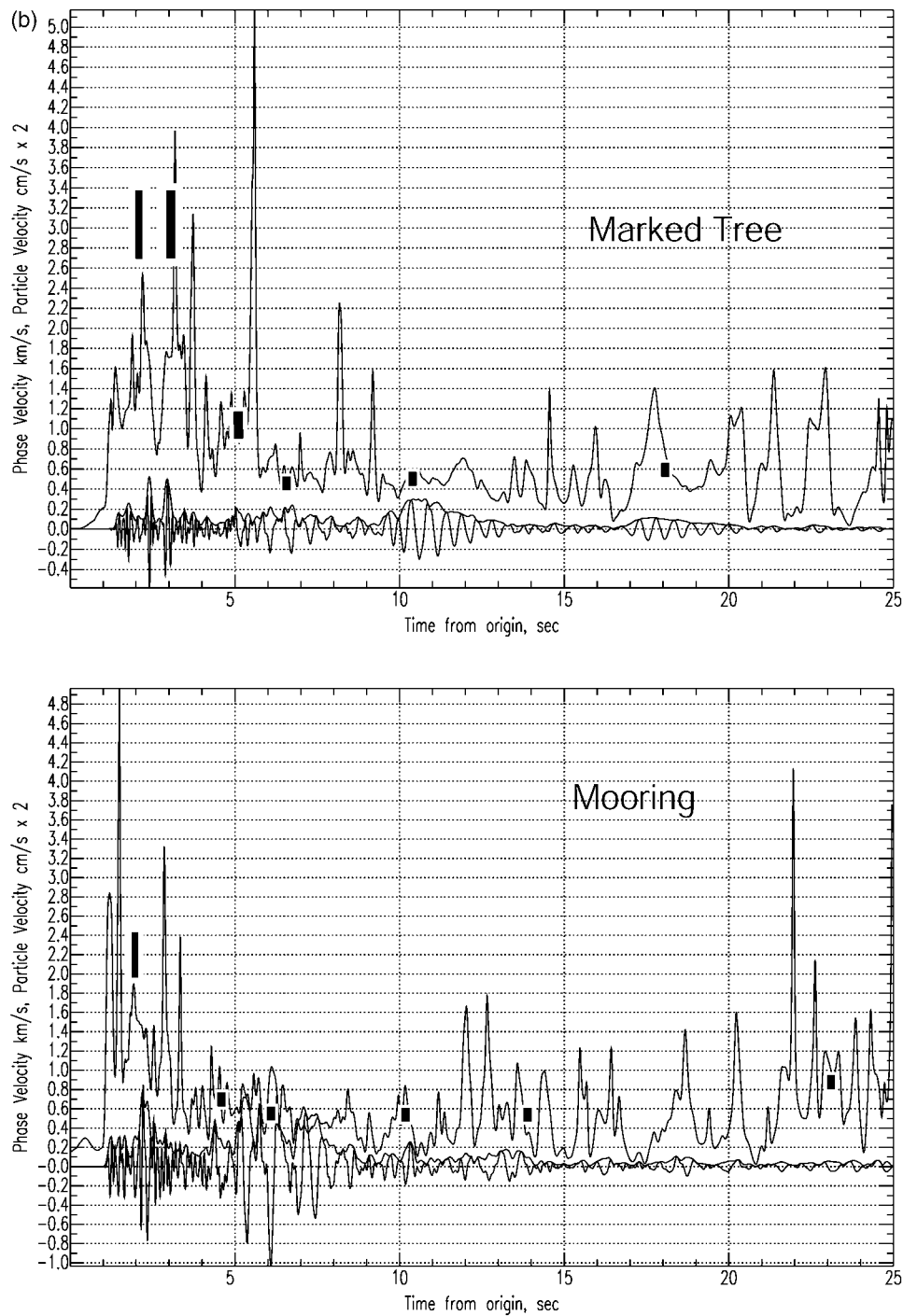


Figure 8. Continued.

Nevertheless, the waveform data from these linear arrays have given a useful glimpse into the nature of strong-motion wave propagation within the thick embayment sediments. First, the data demonstrate that the wave field is understandable. The slow material velocities of the sediments give rise to well-separated body-wave and surface-wave arrivals that travel at velocities related to their mode of propagation. Reflected *P* waves and *PS* conversions have

expected high-phase velocities and long-duration surface waves are dispersed with very low group and phase velocities. To first order, the embayment sediments form an excellent wave guide but also show the effects of velocity heterogeneity in the form of long-duration wave codas and transverse components.

This information has important application to earthquake-engineering considerations. The Mississippi embay-

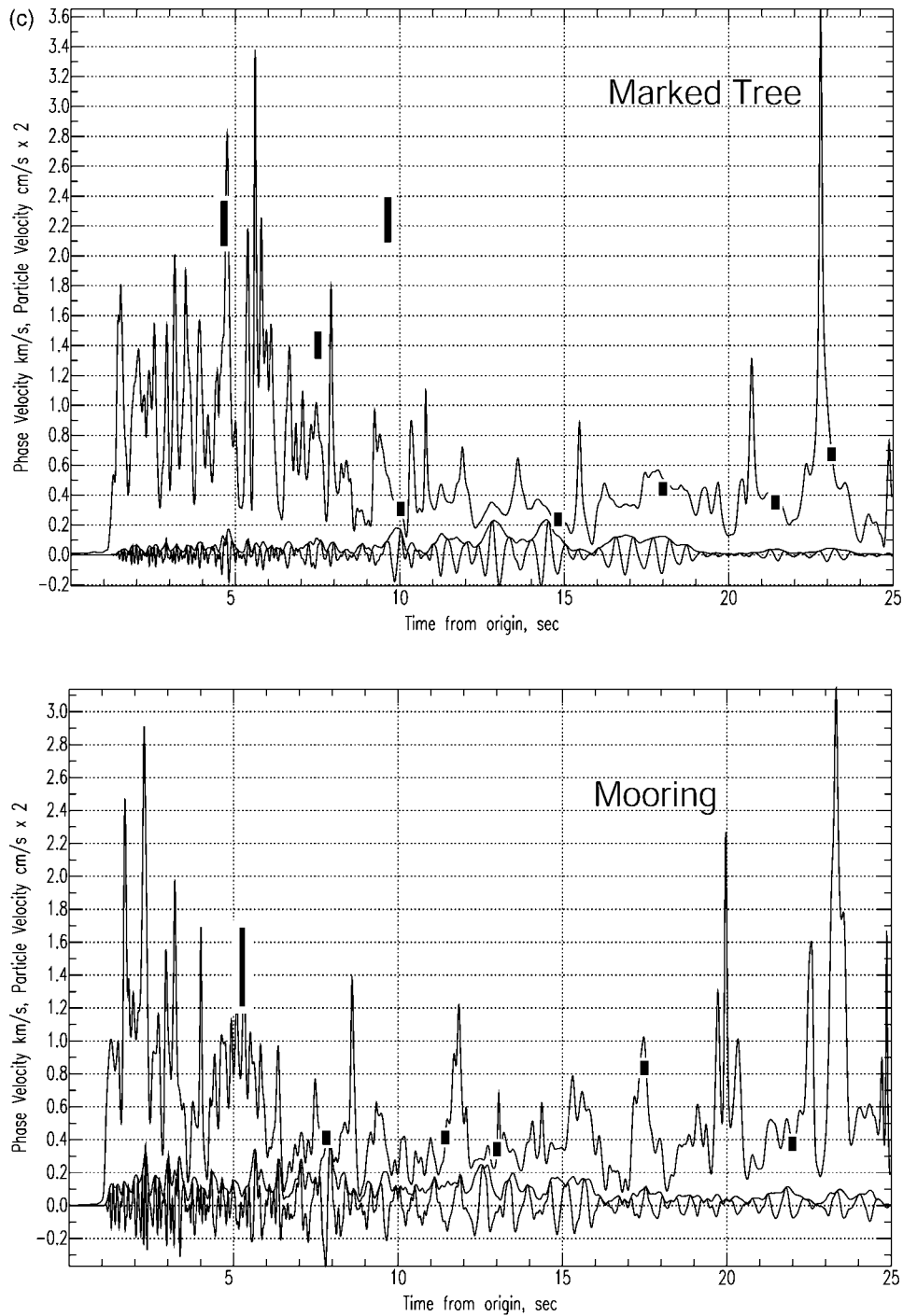


Figure 8. Continued.

ment and related Gulf and southeastern coastal plain provinces are unique seismic structures in North America because of their great lateral extent and because of the existence of at least two major seismic zones, New Madrid and Charleston, South Carolina, within them. We speculate that the combination of a low-velocity seismic wave guide and active seismic zones suggests that strong-motion wave propagation may be more efficient and longer in duration than

occurs in the western United States where earth structure is more heterogeneous. The seismic properties of the wave guide then become very important for evaluating the hazards due to strong ground motions. Langston *et al.* (2005) showed that the attenuation properties of embayment sediments are much less than previously believed, supporting the idea that strong ground motions may propagate to large distances from the source just because of the sedimentary wave guide.

The coherence measurements made from the arrays suggest that high-frequency *S* waves will be relatively incoherent over distance scales as short as 50 m in the embayment. The high-frequency *S*-wave proxies, the radial *PS* conversions in the first 4 sec of record, lose coherence quickly with distance and frequency (Figs. 5b and 6b). Part of the incoherence of these phases is probably because they are produced by a scattering process at the base of the sediments through conversion from the primary *P* wave. The vertical-component *P* wave is observed to be very coherent for both blasts (Fig. 5a and b) even at the highest-frequency accelerations. However, it is likely that high-frequency *S* waves from a local earthquake will be less coherent just because they will need to propagate greater distances from the hypocenter to the surface, encountering even more heterogeneity in the Paleozoic sediments below the unconsolidated embayment sediments and within the crystalline basement rocks. The explosion experiment is too ideal, in a sense, because the wave propagation is largely confined to the unconsolidated sediments. Our results do suggest that the incoherent wave field is a factor for concern in designing large, distributed structures within the embayment and are consistent with results found in other source zones (e.g., Spudich, 1994).

The use of the displacement gradient to estimate horizontal-phase velocity is an interesting by-product of the present analysis. Past studies of geodetic array strain measurements have emphasized the magnitude of strain from strong ground motions as an important seismic wave-field observation that is directly applicable to the response of underground-built structures and for estimating dynamic stress changes (e.g., Spudich *et al.*, 1995; Bodin *et al.*, 1997; Singh *et al.*, 1997; Gomberg *et al.*, 1999). We suggest that analysis of phase velocity from the amplitude of displacement gradients and ground velocity is actually a very useful technique to apply to array data for all sorts of standard seismic experiments. Provided that array sensors have matched responses, the computation of horizontal-phase velocities from displacement gradients can potentially find use in refraction and reflection studies. This technique can produce an additional map of phase velocity as a function of space and time across an array under various assumptions of frequency band that can be used as constraints in structure interpretation. These ideas are left for future development.

Conclusions

Strong ground motions recorded by 100-m linear arrays of accelerographs from large explosions in the Mississippi embayment display a variety of *P*, *PS*, and surface waves that are produced by understandable wave-propagation mechanisms within the low-velocity, unconsolidated sediments. Coherence of these waves was examined by considering the body waves and surface waves in two separate time windows of data. Coherence of displacement, velocity, and acceleration was computed by using the maximum of the normalized cross correlation to examine the progressive degradation of coherence with increasing frequency. Coherence

progressively decreases with ground-motion component type (from vertical to radial to transverse), ground-motion type (from displacement to velocity to acceleration), and with distance between sensors. *PS* conversions are used as a proxy for earthquake *S* waves. The results suggest that high-frequency *S* waves will lose coherence over distances less than 50 m and imply that this will be an important factor for the seismic response of large built structures in the embayment. We also suggest that a technique of determining horizontal-phase velocity from the ratio of the velocity time series to the displacement gradient is a useful way to map phase velocity as a function of space and time that can find use in array analysis, refraction, and reflection experiments.

Acknowledgments

The experimental portion of this work could not have been completed without the help of many people. We appreciate the assistance of Ed Criley and Tom Burdett of the U.S. Geological Survey who helped design the ESEE borehole shot points. Jack Van Schaack and Ron Kaderabek graciously came out of retirement to load and detonate the ESEE explosions. CERI technical personnel Greg Steiner, Jim Bollwerk, Chris McGoldrick, and John Filipic ably managed logistics and helped install field stations during ESEE. We appreciate graduate students Ivan Rabak, Daejin Kang, and Qingwen Miao for their help with instrumentation preparation and installation. Appreciation is given to Charles Glover of the Ritter Land and Seed Co. for their help in siting the Mark Tree, Arkansas, source and to James Eddlemon of Mooring, Tennessee, for help in siting the Mooring source. Kathy Tucker helped produce the graphics for Figure 1. The comments of an anonymous reviewer, Shri Krishna Singh, and associate editor Art McGarr were useful in improving this manuscript. This research was supported by the U.S. Department of the Interior, U.S. Geological Survey under Grant 02HQGR007 and by the National Science Foundation Mid America Earthquake Center under project HD-5. We also thank the University of Memphis for providing seed support through a Faculty Research Grant. Use of the GMT program for Figure 1 (Wessel and Smith, 1998) is gratefully acknowledged. The Seismic Analysis Code (Goldstein and Minner, 1996) was used for much for the analysis.

References

- Abrahamson, N. A. (1991). Empirical spatial coherency functions for application to soil-structure interaction analyses, *Earthquake Spectra* **7**, 1–28.
- Abrahamson, N. A., B. A. Bolt, R. B. Darragh, J. Penzien, and Y. B. Tsai (1987). The SMART-I accelerograph array (1980–1987): a review, *Earthquake Spectra* **3**, 263–287.
- Barker, J. S., M. Campillo, F. J. Sanchez-Sesma, D. Jongmans, and S. K. Singh (1996). Analysis of wave propagation in the valley of Mexico from a dense array of seismometers, *Bull. Seism. Soc. Am.* **86**, 1667–1680.
- Bodin, P., and S. Horton (1999). Broadband microtremor observation of basin resonance in the Mississippi embayment, central U.S.: implications for seismic hazard assessment, *Geophys. Res. Lett.* **26**, 903–906.
- Bodin, P., J. Gomberg, S. K. Singh, and M. Santoyo (1997). Dynamic deformations of shallow sediments in the Valley of Mexico, part I: three-dimensional strains and rotations recorded on a seismic array, *Bull. Seism. Soc. Am.* **87**, 528–539.
- Bracewell, R. N. (1978). *The Fourier Transform and Its Applications*, McGraw-Hill Book Company, New York.
- Chen, K., J. Chiu, and Y. Yang (1996). Shear-wave velocity of the sedimentary basin in the upper Mississippi embayment using S-to-P converted waves, *Bull. Seism. Soc. Am.* **86**, 848–856.

- Chiu, J. M., A. C. Johnston, and Y. T. Yang (1992). Imaging the active faults of the central New Madrid seismic zone using Panda array data, *Seism. Res. Lett.* **63**, 375–393.
- Farnbach, J. S. (1975). The complex envelope in seismic signal analysis, *Bull. Seism. Soc. Am.* **65**, 951–962.
- Goldstein, P., and L. Minner (1996). SAC2000: seismic signal processing and analysis tools for the 21st century, *Seism. Res. Lett.* **67**, 39.
- Gomberg, J., G. Pavlis, and P. Bodin (1999). The strain in the array is mainly in the plane (waves below ~ 1 Hz), *Bull. Seism. Soc. Am.* **89**, 1428–1438.
- Harichandran, R. S., and E. H. Vanmarcke (1986). Stochastic variation of earthquake ground motion in space and time, *J. Eng. Mech., ASCE* **112**, no. 2, 154–174.
- Helmberger, D. V. (1983). Theory and application of synthetic seismograms, in *Earthquakes: Observations, Theory and Interpretation*, H. Kanamori and E. Boschi (Editors), North Holland for the Italian Physical Society, Amsterdam.
- Johnston, A. C., and E. S. Schweig (1996). The enigma of the New Madrid earthquakes of 1811–1812, *Annu. Rev. Earth. Planet. Sci.* **24**, 339–384.
- Kramer, S. L. (1996). *Geotechnical Earthquake Engineering*, Prentice Hall, Upper Saddle River, New Jersey.
- Langston, C. A. (2003). Local earthquake wave propagation through Mississippi Embayment sediments: I. body wave phases and local site responses, *Bull. Seism. Soc. Am.* **93**, 2664–2684.
- Langston, C. A., P. Bodin, C. Powell, M. Withers, S. Horton, and W. Mooney (2005). Bulk sediment Qp and Qs in the Mississippi embayment, Central U.S., *Bull. Seism. Soc. Am.* **95**, 2162–2179.
- Langston, C. A., W. Mooney, P. Bodin, C. Powell, and M. Withers (2002a). Experiment in New Madrid Zone to employ active source, *EOS Trans. AGU* **83**, 473.
- Langston, C. A., C. A. Powell, and G. Patterson (2002b). Strong ground motion in the New Madrid seismic zone and lifeline vulnerability, in *Proceedings of the Fourth China-Japan-USA Trilateral Symposium on Lifeline Earthquake Engineering*, S. T. Y. Hu and A. S. Kiremidjian (Editors), Qindao, China.
- Lanzo, G., and M. Vucetic (1999). Effect of soil plasticity on damping ratio at small cyclic strains, *Soils Foundations Jpn. Tech. Soc.* **39**, 131–141.
- Liu, H., Y. Hu, J. Dorman, T. Chang, and J. Chiu (1997). Upper Mississippi embayment shallow seismic velocities measured in situ, *Eng. Geol.* **46**, 313–330.
- Love, A. E. H. (1927). *A Treatise on the Mathematical Theory of Elasticity*, Fourth Ed., Dover Publications, New York.
- Nuttli, O. W. (1973). The Mississippi Valley earthquakes of 1811 and 1812: intensities, ground motions, and magnitudes, *Bull. Seism. Soc. Am.* **63**, 227–248.
- Self, R. P. (1993). Late Tertiary to early Quaternary sedimentation in the Gulf coastal plain and lower Mississippi valley, *Southeast. Geol.* **33**, 99–110.
- Singh, S. K., M. Santoyo, P. Bodin, and J. Gomberg (1997). Dynamic deformations of shallow sediments in the Valley of Mexico, part II: single-station estimates, *Bull. Seism. Soc. Am.* **87**, 540–550.
- Spudich, P. (1994). Recent seismological insights into the spatial variation of earthquake ground motions, in *Proceedings of Seminar on New Developments in Earthquake Ground Motion Estimation and Implications for Engineering Design Practice*, Applied Technology Council ATC 35-1, Redwood City, California.
- Spudich, P., L. K. Steck, M. Hellweg, J. B. Fletcher, and L. M. Baker (1995). Transient stresses at Parkfield, California, produced by the M7.4 Landers earthquake of June 28, 1992: observations from the UPSAR dense seismograph array, *J. Geophys. Res.* **100**, 675–690.
- Stearns, R. G. (1957). Cretaceous, Paleocene, and lower Eocene geologic history of the northern Mississippi embayment, *Geol. Soc. Am. Bull.* **68**, 1077–1100.
- Stearns, R. G., and M. V. Marcher (1962). Late Cretaceous and subsequent structural development of the northern Mississippi embayment area, *Geol. Soc. Am. Bull.* **73**, 1387–1394.
- Tuttle, M. P., and E. S. Schweig (1999). Towards a paleoearthquake chronology for the New Madrid seismic zone, *U.S. Geol. Surv. NEHRP Ann. Rept.*, 17 p.
- Vucetic, M. (1994). Cyclic threshold shear strains in soils, *J. Geotech. Eng.* **120**, 2208–2228.
- Wessel, P., and W. H. F. Smith (1998). New, improved version of Generic Mapping Tools released, *EOS Trans. AGU* **79**, 579.
- Zerva, A., and V. Zervas (2002). Spatial variation of seismic ground motions: an overview, *Appl. Mech. Rev.* **55**, no. 3, 271–297.

Appendix

This is a short proof showing that equation (2) is equivalent to a standard way of computing coherence by using the spectral coherency.

The Power theorem relating time- and frequency-domain representations of two functions, f and g , is given by Bracewell (1975) as

$$\int_{-\infty}^{+\infty} f(t)g(t) dt = \int_{-\infty}^{+\infty} F(\omega)G^*(\omega) d\omega, \quad (\text{A1})$$

where $F(\omega)$ and $G(\omega)$ are the complex Fourier spectra of f and g , and the $*$ denotes the complex conjugate of the function. The normalized cross correlation is

$$\phi(\tau) = \frac{\int_{-\infty}^{+\infty} f(t)g(t + \tau) dt}{\sqrt{\int_{-\infty}^{+\infty} f^2(t) dt} \sqrt{\int_{-\infty}^{+\infty} g^2(t) dt}}. \quad (\text{A2})$$

By Raleigh's theorem (Bracewell, 1975) we have, for example,

$$\sqrt{\int_{-\infty}^{+\infty} f^2(t) dt} = \sqrt{\int_{-\infty}^{+\infty} F(\omega)F^*(\omega) d\omega}. \quad (\text{A3})$$

Dividing equation (A1) by the left- and right-hand sides of (A3), respectively, for both f and g gives

$$\begin{aligned} & \frac{\int_{-\infty}^{+\infty} f(t)g(t) dt}{\sqrt{\int_{-\infty}^{+\infty} f^2(t) dt} \sqrt{\int_{-\infty}^{+\infty} g^2(t) dt}} \\ &= \frac{\int_{-\infty}^{+\infty} F(\omega)G^*(\omega) d\omega}{\sqrt{\int_{-\infty}^{+\infty} F(\omega)F^*(\omega) d\omega} \sqrt{\int_{-\infty}^{+\infty} G(\omega)G^*(\omega) d\omega}}. \quad (\text{A4}) \end{aligned}$$

We substitute the lagged function $g(t + \tau)$ into equation (A4) and note that the complex conjugate of its spectrum is, by the shift theorem,

$$\mathcal{T}[g(t + \tau)]^* = G^*(\omega)e^{-i\omega\tau} \quad (\text{A5})$$

and take the maximum of both sides to get the definition of equation (2) in terms of the Fourier transforms of the individual time series

$$C_{xy} = \max \frac{\int_{-\infty}^{+\infty} f(t)g(t + \tau)dt}{\sqrt{\int_{-\infty}^{+\infty} f^2(t)dt} \sqrt{\int_{-\infty}^{+\infty} g^2(t)dt}} \quad (\text{A6})$$

$$= \max \frac{\int_{-\infty}^{+\infty} F(\omega)G^*(\omega)e^{-i\omega\tau}d\omega}{\sqrt{\int_{-\infty}^{+\infty} F(\omega)F^*(\omega)d\omega} \sqrt{\int_{-\infty}^{+\infty} G(\omega)G^*(\omega)d\omega}}.$$

The maximum normalized cross correlation will occur for some τ_{\max} . Equation (A6) is exactly a representation of the coherence implied by equation (1) if spectral averaging is performed over the entire frequency band (signified by the spectral integrations). In a sense, this is an unbiased way to perform the spectral averaging because the entire band is chosen. However, in practice, we window seismic phases in the time domain to isolate them, then find the maximum of the normalized cross correlation. Bias occurs through the choice of time window but not the choice of frequency band.

Center for Earthquake Research and Information
University of Memphis
Memphis, Tennessee 38152
(C.A.L., P.B., C.P., M.W., S.H.)

U.S. Geological Survey
345 Middlefield Road
Menlo Park, California 91125
(W.M.)

Manuscript received 18 May 2005.